Analysis of light propagation in slotted resonator based systems via coupled-mode theory

Kirankumar R. Hiremath,[1,*] **Jens Niegemann,**[2,3] **and Kurt Busch**[2,4]

[1]*Department of Mathematics, Karlsruhe Institute of Technology (KIT), Germany*
[2]*Institut für Theoretische Festkörperphysik and DFG-Center for Functional Nanostructures (CFN), Karlsruhe Institute of Technology (KIT), Germany*
[3]*jens.niegemann@kit.edu*
[4]*kurt.busch@kit.edu*
[*]*hiremath@math.uni-karlsruhe.de*

Abstract: Optical devices with a slot configuration offer the distinct feature of strong electric field confinement in a low refractive index region and are, therefore, of considerable interest in many applications. In this work we investigate light propagation in a waveguide-resonator system where the resonators consist of slotted ring cavities. Owing to the presence of curved material interfaces and the vastly different length scales associated with the sub-wavelength sized slots and the waveguide-resonator coupling regions on the one hand, and the spatial extent of the ring on the other hand, this prototypical system provides significant challenges to both direct numerical solvers and semi-analytical approaches. We address these difficulties by modeling the slot resonators via a frequency-domain spatial Coupled-Mode Theory (CMT) approach, and compare its results with a Discontinuous Galerkin Time-Domain (DGTD) solver that is equipped with curvilinear finite elements. In particular, the CMT model is built on the underlying physical properties of the slotted resonators, and turns out to be quite efficient for analyzing the device characteristics. We also discuss the advantages and limitations of the CMT approach by comparing the results with the numerically exact solutions obtained by the DGTD solver. Besides providing considerable physical insight, the CMT model thus forms a convenient basis for the efficient analysis of more complex systems with slotted resonators such as entire arrays of waveguide-coupled resonators and systems with strongly nonlinear optical properties.

OCIS codes: (130.3120) Integrated optics devices; (230.5750) Resonators; (130.6010) Sensors; (000.4430) Numerical approximation and analysis; (000.3860) Mathematical methods in physics.

References and links

1. A. Taflove and S. C. Hagness, *Computational Electrodynamics: The Finite Difference Time Domain Method*, 3rd ed. (Artech House Inc., 2005).
2. J. Jin, *The Finite Element Method in Electromagnetics*, 2nd ed. (Wiley-Interscience Publication, 2002).
3. G. W. Pan, *Wavelets in Electromagnetics and Device Modeling*, Microwave and Optical engineering, (Wiley Interscience, 2003).
4. J. S. Hesthaven and T. Warburton, *Nodal Discontinuous Galerkin Methods: Algorithms, Analysis, and Applications*, Number 54 in Texts in Applied Mathematics, (Springer-Verlag, 2007).

#141007 - $15.00 USD
Received 13 Jan 2011; accepted 11 Mar 2011; published 19 Apr 2011

5. J. Niegemann, M. König, K. Stannigel, and K. Busch, "Higher-order time-domain methods for the analysis of nano-photonic systems," Photon. Nanostr.: Fundam. Appl. **7**(1), 2–11 (2009).
6. J. Niegemann, W. Pernice, and K. Busch, "Simulation of optical resonator using DGTD and FDTD," IOP J. Opt. A: Pure Appl. Opt. **11**, 114015:1–10 (2009).
7. K. Stannigel, M. König, J. Niegemann, and K. Busch, "Discontinuous Galerkin time-domain computations of metallic nanostructures,, Opt. Express **17**(17), 14934–14947 (2009).
8. B. E. Little, S. T. Chu, H. A. Haus, J. Foresi, and J. P. Laine. "Microring resonator channel dropping filters," J. Lightwave Technol. **15**(6), 998–1005 (1997).
9. J. V. Hryniewicz, P. P. Absil, B. E. Little, R. A. Wilson, and P.-T. Ho, "Higher order filter response in coupled microring resonators," IEEE Photon. Technol. Lett. **12**(3), 320–322 (2000).
10. H. G. Rabus, M. Hamacher, U. Troppenz, and H. Heidrich, "High-Q channel-dropping filters using ring resonators with integrated SOAs," IEEE Photon. Technol. Lett. **14**(10), 1442–1444 (2002).
11. A. Melloni, R. Costa, P. Monguzzi, and M. Martinelli, "Ring-resonator filters in silicon oxynitride technology for dense wavelength-division multiplexing systems," Opt. Lett. **28**(17), 1567–1569 (2003).
12. C. K. Madsen, G. Lenz, A. J. Bruce, M. A. Capuzzo, L. T. Gomez, T. N. Nielsen, and I. Brener, "Multistage dispersion compensator using ring resonators," Opt. Lett. **24**(22), 1555–1557 (1999).
13. A. M. Armani and K. J. Vahala, "Heavy water detection using ultra-high-Q microcavities," Opt. Lett. **31**(12), 1896–1898 (2006).
14. S. Pereira, P. Chak, S. E. Sipe, L. Tkeshelashvili, and K. Busch, "All-optical diode in an asymmetrically apodized kerr nonlinear microresonator system," Photon. Nanostr.: Fundam. Appl. **2**, 181–190 (2004).
15. V. R. Almeida, Q. Xu, C. A. Barios, and M. Lipson, "Guiding and confining light in void nanostructure," Opt. Lett. **29**(11), 1209–1211 (2004).
16. C. Koos, P. Vorreau, T. Vallaitis, P. Dumon, W. Bogaerts, R. Baets, B. Esembeson, I. Biaggio, T. Michinobu, F. Diederich, W. Freude, and J. Leuthold, "All-optical high-speed signal processing with silicon-organic hybrid slot waveguides," Nat. Photonics **2**(3), 216–219 (2009).
17. T. Baehr-Jones, M. Hochberg, C. Walker, and A. Scherer. "High-Q optical resonators in silicon-on-insulator-based slot waveguides," Appl. Phys. Lett. **86**, 081101 (2005).
18. T. Baehr-Jones, M. Hochberg, G. Wang, R. Lawson, Y. Liao, P. Sullivan, L. Dalton, A. Jen, and A. Scherer, "Optical modulation and detection in slotted silicon waveguides," Opt. Express **13**(14), 5216–5226 (2005).
19. K. R. Hiremath, "Analytical modal analysis of bent slot waveguides," J. Opt. Soc. Am. A **26**(11), 2321–2326 (2009).
20. X. Ji, T. Lu, W. Cai, and P. Zhang, "Discontinuous Galerkin Time Domain (DGTD) methods for the study of 2-D waveguide-coupled microring resonators," J. Lightwave Technol. **23**(11), 3864–3874 (2005).
21. K. R. Hiremath, R. Stoffer, and M. Hammer, "Modeling of circular integrated optical microresonators by 2-D frequency domain coupled mode theory," Opt. Commun. **257**, 277–297 (2006).
22. K. R. Hiremath, *Coupled mode theory based modeling and analysis of circular optical microresonators*, PhD thesis, University of Twente, The Netherlands (2005).
23. M. Hammer, K. R. Hiremath, and R. Stoffer, "Analytical approaches to the description of optical microresonator devices," in F. Michelotti, A. Driessen, and M. Bertolotti, editors, *Microresonators as building blocks for VLSI photonics*, volume 709 of AIP conference proceedings, pages 48–71. American Institute of Physics, Melville, New York (2004).
24. K. R. Hiremath, M. Hammer, S. Stoffer, L. Prkna, and J. Čtyroký, "Analytic approach to dielectric optical bent slab waveguides," Opt. Quantum Electron. **37**(1–3), 37–61 (2005).
25. T. Tamir, editor, *Integrated Optics (Second Corrected and Updated Edition)*, Topics in Applied Physics, vol. 7, (Springer-Verlag, 1982).
26. A. Ghatak and K. Thyagarajan, *Optical Electronics* (Cambridge University Press, 1993).
27. A. F. Oskooi, D. Roundy, M. Ibanescu, P. Bermel, J. D. Joannopoulos, and S. G. Johnson, "Meep: A flexible free-software package for electromagnetic simulations by the FDTD method," Comput. Phys. Commun. **181**(3), 687–702 (2010).
28. R. Stoffer, K. R. Hiremath, M. Hammer, L. Prkna, and J. Čtyroký, "Cylindrical integrated optical microresonators: Modeling by 3-D vectorial coupled mode theory," Opt. Commun. **256**, 46–67 (2005).

1. Introduction

A popular strategy for solving Maxwell's equations for a system with complex geometries and/or material response is to develop flexible and versatile all-purpose methods that allow for their direct numerical solution. Classic examples of this approach include the venerable and well-established Finite-Difference Time-Domain method [1] and the standard Finite Element method [2], both of which are continuously further developed and refined. Modern all-purpose approaches include wavelet-based methods [3] and Discontinuous Galerkin Time-

#141007 - $15.00 USD Received 13 Jan 2011; accepted 11 Mar 2011; published 19 Apr 2011

Domain methods [4–7]. These generic methods are applied to a huge variety of physical settings such as linear and nonlinear optical wave propagation in waveguides, periodic structures, and various scattering problems etc. Clearly, the price that has to be paid for such versatility is that for certain classes of optical systems these methods become computationally rather expensive and provide only limited insight into the underlying physical mechanisms.

Coupled waveguide-resonator systems represent one such particularly important class of optical devices. In these systems, optical resonators such as circular micro-resonators (see Fig. 1) provide a discrete set of resonances with high quality factors (Q) that allow for the efficient trapping of electromagnetic energy. This unique property may be exploited for a number of applications. For instance, the discrete nature of these resonances lend themselves for the realization of compact filtering and multiplexing devices [8–11] and their dispersive properties find use in dispersion compensation schemes [12]. Furthermore, these resonances are very sensitive to the dielectric environment and may, therefore, be utilized for advanced sensing purposes [13]. In addition, low-power nonlinear-optical devices such as optical diodes based on arrays of coupled waveguide-resonator systems have been suggested [14]. The physical reason for these effects lies in the fact that these devices are extremely sensitive to the phase of the light field. From a modeling point of view this means that errors in the spatial discretization and/or the time-stepping can easily lead to inaccurate and even unphysical results. As a result, efficient and reliable simulations of coupled waveguide-resonator systems still represent a challenge for direct numerical methods.

The situation becomes particularly demanding for the simulation of light propagation in slotted resonators such as those depicted in Fig. 1. Such slotted configurations exploit the fact that the introduction of a sub-wavelength slot in conventional ridge/slab waveguides leads — for an appropriately polarized mode — to an extremely high electric field confinement inside the (low-refractive index) slot region [15]. This property originates from the discontinuity of the normal component of the electric field across material interfaces. The resulting strong field confinement can be exploited by depositing highly nonlinear low-index material within the slot region [16]. Moreover, by introducing such sub-wavelength slots into traditional resonator structures, it becomes possible to combine the field enhancement inside the slot with the resonance trapping effect discussed above. This allows one to boost further the resonance field enhancement. As a matter of fact, such slotted resonators have already been utilized for novel sensing applications [17] as well as low-power optical modulation and detection [18]. In view of the dramatic improvements in nano-scale fabrication, it is expected that slotted waveguide and slotted resonator systems will develop into a novel platform for high-performance integrated optics.

An analysis of curved slotted waveguides has shown that the position of the slot inside the guiding core greatly influences the modal field properties of the waveguide [19]. Correspondingly, all parameters of practical interest such as bending loss, peak field localization, power confinement in various regions of the waveguide etc. sensitively depend on the position of the slot. Therefore, we expect that when a slot is introduced into an ordinary micro-ring resonator, its position strongly affects the resonance frequencies and the associated Q-factors of the resonator. From a modeling point of view, coupled waveguide-resonator systems, where the resonators consists of slotted ring cavities thus provide a particularly challenging class of optical systems. For instance, a numerical solver must keep under control not only any spatial discretization errors in the representation of curved surfaces and efficiently resolve the sub-wavelength slot, but must also be able to consistently handle the discontinuities in the fields. We will demonstrate below that a Discontinuous Galerkin Time-Domain (DGTD) method [5–7, 20] enhanced with curvilinear finite elements [4] is able to address these challenges in a satisfactory manner.

#141007 - $15.00 USD Received 13 Jan 2011; accepted 11 Mar 2011; published 19 Apr 2011

However, even such sophisticated computational tools require long simulation times, therefore it makes perfect sense to develop a dedicated semi-analytical model that takes into account the characteristic physical properties of the resonators and waveguides under consideration. As a matter of fact, coupled-mode theory (CMT) is an established semi-analytical tool in the area of integrated optics. For instance, it has been shown that the frequency-domain CMT-based modeling of ordinary resonators provides a very accurate method that yields further insight into the operation principles of conventional resonator-based devices [21]. Using the semi-analytic modal solutions of the bent slotted waveguides [19], in the present paper we extend the CMT approach to the modeling of slotted resonator systems. More precisely, by developing such a CMT-based model, we capture the essence of the physical problem with reduced complexity, and without 'much' loss of accuracy. Of course, just how 'much' loss of accuracy we incur has to be determined by comparison with exact numerical solutions - in our case, DGTD equipped with curvilinear elements. Once we have established the CMT model and the corresponding limitations, we can push ahead and conduct parameter scans and investigate entire arrays of coupled waveguide-resonator systems with slot configurations.

Consequently, in Sec. 2 we describe the CMT formulation of slotted resonator systems by taking into account the interaction between a finite number of guided modes of straight coupling waveguides and a finite number of modes of bent slotted waveguides. We present the simulation results of this model in Sec. 3, where we also validate the applicability of the CMT approach for the slotted resonator systems by comparing with the results of exact DGTD computations. In Sec. 4 we conclude with a discussion of these results, comment on the insights provided by our CMT approach, and discuss potential further developments.

2. CMT model of slotted resonators

In Fig. 1, we depict a prototypical slotted micro-ring resonator that is coupled to two straight waveguides. Clearly, while other configurations such as coupling to a single straight waveguide or to slotted waveguides as well as several coupled slotted resonators could be considered, they do not present any further conceptual difficulties so that we will, in this work, restrict ourselves to an exposition of the CMT approach for the above model system.

2.1. Overall device description

As seen from a device point of view, this coupled slotted-resonator waveguide system exhibits two input ports (In-port and Add-port), and two output ports (Through-port and Drop-port). The operating principle of this device is based on the coupling of the fields in the straight waveguides to the cavity modes provided by the slotted resonator, and the subsequent interference between these excited cavity modes with the fields in the various waveguides [22].

In what follows, we work in the frequency-domain and limit ourselves to a linear optics setting [23]. Within this standard approach, the waveguides-coupled slotted resonator is conceptually divided into two bent-straight waveguide couplers (the boxes (I) and (II) delineated by dashed lines in Fig. 1) together with appropriate connections between the couplers via segments of bent slotted waveguides. In addition, the individual couplers are connected to the input and output ports described above, which are realized via straight waveguides. We assume that couplers (I) and (II) are adiabatic so that back-reflections into the bent slotted waveguide segments and straight waveguide ports can be neglected. This allows us to consider only uni-directional wave propagation as indicated by the white arrows in Fig. 1. Clearly, this is one of the major assumptions of coupled-mode theory whose validity has to be checked by a subsequent comparison with exact numerical simulations.

The couplers (I) and (II) represent finite interaction regions and outside these regions we assume that the fields in the associated waveguides (bent slotted waveguides segments and

#141007 - $15.00 USD Received 13 Jan 2011; accepted 11 Mar 2011; published 19 Apr 2011

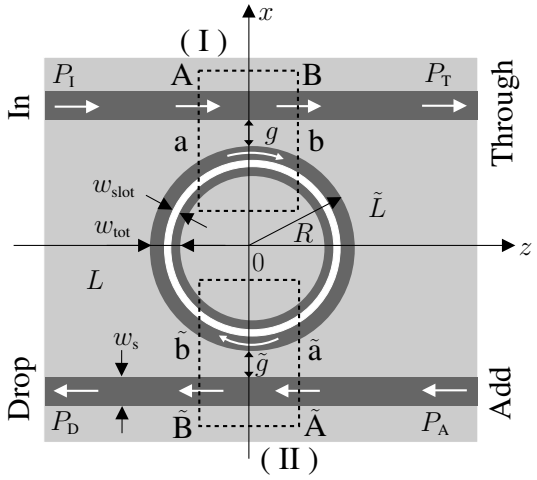

Fig. 1. Schematics for a slotted-resonator based 4-port device. The resonator consists of a ring of outer radius R, width $w_{\rm tot}$, and refractive index $n_{\rm c}$, and contains a low-index slot of width $w_{\rm slot}$ and refractive index $n_{\rm slot} < n_{\rm c}$. The slot's position inside the ring is described by the asymmetry parameter η such that the width of the inner high-index ring layer is ηw and that of the outer high-index ring layer is $(1-\eta)w$, where $w = w_{\rm tot} - w_{\rm slot}$ [19]. This slotted resonator is coupled to two identical straight waveguides of width $w_{\rm s}$ and refractive index $n_{\rm s}$ that realize input and output ports. The minimal separation between resonator and the straight waveguides are g and $\tilde{g}$, respectively. The entire device is embedded in a host material with a background index n_b and its performance may be characterized via the power levels associated with the input ports, $P_{\rm I}$ and $P_{\rm A}$ (In- and Add-port), and the output ports, $P_{\rm T}$ and $P_{\rm D}$ (Through- and Drop-port), respectively. Within a coupled-mode theoretical approach this device is further decomposed into several functional elements. Two couplers, (I) and (II), delineated with dashed-line boxes, are connected via two identical segments of bent slotted waveguides of length L and $\tilde{L}$ (at positions a, b, and ã, b̃, respectively) and each of these couplers is further connected to two identical input and output port waveguides (at positions A, B, and Ã, B̃, respectively).

straight waveguides ports) are uncoupled, i.e., that we may represent the fields through the freely propagating modes associated with these waveguides. For definiteness and without loss of generality, let us suppose that the bent slotted waveguides supports $N_{\rm b}$ guided modes, and the straight waveguides support $N_{\rm s}$ guided modes and that these modes are power normalized [24, Sec. 2.1], [25, Sec. 2.2.6].

In general, the response of the couplers can be characterized by the coupler scattering matrices S and $\tilde{\mathsf{S}}$ for couplers (I) and (II), respectively, as

$$\begin{pmatrix} b \\ B \end{pmatrix} = \mathsf{S} \begin{pmatrix} a \\ A \end{pmatrix}, \qquad \begin{pmatrix} \tilde{b} \\ \tilde{B} \end{pmatrix} = \tilde{\mathsf{S}} \begin{pmatrix} \tilde{a} \\ \tilde{A} \end{pmatrix}. \tag{1}$$

In the above expressions A, B, and a, b are amplitude vectors of lengths $N_{\rm s}$ and $N_{\rm b}$, respectively, that correspond to properly normalized 'forward' propagating guided modes at the respective positions A, B, a, and b related to coupler (I). Here, for straight waveguides, the forward direction is defined as propagating from input to output port; whereas for the bent slotted waveguide segments, the 'forward' direction is defined as the clockwise direction (cf. Fig. 1). Analogous statements apply to the amplitude vectors $\tilde{A}$, $\tilde{B}$, $\tilde{a}$, and $\tilde{b}$ pertaining to coupler (II).

For the subsequent analysis, it is advantageous to represent these abstract scattering matrices

#141007 - $15.00 USD Received 13 Jan 2011; accepted 11 Mar 2011; published 19 Apr 2011

according to

$$\mathsf{S} = \begin{pmatrix} \mathsf{S}_{\mathrm{bb}} & \mathsf{S}_{\mathrm{bs}} \\ \mathsf{S}_{\mathrm{sb}} & \mathsf{S}_{\mathrm{ss}} \end{pmatrix}, \qquad \tilde{\mathsf{S}} = \begin{pmatrix} \tilde{\mathsf{S}}_{\mathrm{bb}} & \tilde{\mathsf{S}}_{\mathrm{bs}} \\ \tilde{\mathsf{S}}_{\mathrm{sb}} & \tilde{\mathsf{S}}_{\mathrm{ss}} \end{pmatrix}, \tag{2}$$

where the sub-matrices S_{vw} represent the coupling of mode $\mathrm{w} \in \{\mathrm{b},\mathrm{s}\}$ to mode $\mathrm{v} \in \{\mathrm{b},\mathrm{s}\}$ and the indices b,s label the different classes of modes, i.e., the index b refers to the modes of the bent slotted waveguide segments and the index s refers to the modes of the straight input- and output-port waveguides.

Outside the coupler regions, the field propagating along the ring segments is described by the bent slotted waveguide guided modes with their angular dependence given by the corresponding mode propagation constants. These complex-valued propagation constants also take into account the radiation loss due to bending [19]. As a result, we obtain

$$a = \mathsf{G}\tilde{b} \quad \text{and} \quad \tilde{a} = \tilde{\mathsf{G}}b, \tag{3}$$

where G and $\tilde{\mathsf{G}}$ are $N_{\mathrm{b}} \times N_{\mathrm{b}}$ diagonal matrices with entries $\mathsf{G}_{p,p} = \exp(-\mathrm{i}\gamma_{\mathrm{b}p}L)$, $\tilde{\mathsf{G}}_{p,p} = \exp(-\mathrm{i}\gamma_{\mathrm{b}p}\tilde{L})$ for $p = 1,\ldots,N_{\mathrm{b}}$, and L and $\tilde{L}$ are the lengths of the bent slotted waveguide segments (cf. Fig. 1). Here $\gamma_{\mathrm{b}p} = \beta_{\mathrm{b}p} - \mathrm{i}\alpha_{\mathrm{b}p}$, $p = 1,\ldots,N_{\mathrm{b}}$, denote the complex-valued propagation constants of the bent slotted waveguide modes with corresponding phase and attenuation constants, $\beta_{\mathrm{b}p}$ and $\alpha_{\mathrm{b}p}$, respectively.

If we specify the amplitudes of the input waveguides, A_q and $\tilde{A_q}$, $q = 1,\ldots,N_{\mathrm{s}}$, we can regard Eqs. (1), (2), and (3) as a system of linear equations for the amplitudes of the output waveguide, B_q and $\tilde{B_q}$, $q = 1,\ldots,N_{\mathrm{s}}$. In particular, if only the In-port waveguide feeds the system, i.e., $\tilde{A_q} \equiv 0$, $q = 1,\ldots,N_{\mathrm{s}}$, we obtain for the amplitudes in the Through- and Drop-port waveguides

$$\left.\begin{aligned} B &= (\mathsf{S}_{\mathrm{sb}}\mathsf{G}\tilde{\mathsf{S}}_{\mathrm{bb}}\tilde{\mathsf{G}}\Omega^{-1}\mathsf{S}_{\mathrm{bs}} + \mathsf{S}_{\mathrm{ss}})A, \\ \tilde{B} &= (\tilde{\mathsf{S}}_{sb}\tilde{\mathsf{G}}\Omega^{-1}\mathsf{S}_{\mathrm{bs}})A, \end{aligned}\right\} \tag{4}$$

where $\Omega = \mathsf{I} - \mathsf{S}_{\mathrm{bb}}\mathsf{G}\tilde{\mathsf{S}}_{\mathrm{bb}}\tilde{\mathsf{G}}$.

Based on Eqs. (4), we can compute the overall spectral device characteristics, once the scattering matrices S, $\tilde{\mathsf{S}}$, and the cavity propagation constants $\gamma_{\mathrm{b}p}$, $p = 1,\ldots,N_{\mathrm{b}}$ are available as a function of the wavelength λ. By using semi-analytic arguments based on modal descriptions of the bent slotted and straight waveguides, we can determine these parameters from first principles as described in the following subsections.

At this point, we would like to note that the above overall device description based on the functional decomposition of the resonator is valid for both two-dimensional and three-dimensional settings. In order to avoid a cluttered notation, we will restrict ourselves in the following to an analysis of the two-dimensional setting, i.e., to the case of propagation in xz-plane as indicated in Fig. 1 without any variation of the material and structural parameters along the y-axis. We comment on the extension to the fully three-dimensional setting in Sec. 4.

2.2. Bent slotted waveguide modes

For the two-dimensional setting described above, Maxwell's curl equations decouple into two sets of equations, one for the so-called transverse-electric (TE) and one for the so-called transverse-magnetic (TM) polarization [24]. As we are chiefly interested in working with electric field enhancement effects within the slot, we consider the case of TM-polarized radiation. For this polarization, the y-component of the magnetic field (H_y) and the in-plane components of the electric field (E_x, E_z) — in the Cartesian co-ordinate system — or (E_r, E_θ) — in the polar co-ordinate system — have to be considered. Clearly, as the normal component of the dielectric displacement field is continuous across a material interface, we have for a bent slotted

#141007 - $15.00 USD Received 13 Jan 2011; accepted 11 Mar 2011; published 19 Apr 2011

waveguide that the radial component of the electric field (E_r) exhibits concurrent jumps from low to high values as the radial position is scanned across jumps from high-index to a low-index materials and vice versa (see Fig. 4).

We determine the required propagation constants for TM-polarized modes in bent slotted waveguides with constant curvature via the analytical model presented in Ref. [19]. Within this approach, we represent the fields in each of the piecewise constant refractive index regions in terms of appropriate Bessel/Hankel functions. Using the boundary conditions of the fields at the material interfaces together with bounded, outgoing wave boundary conditions at infinity, we obtain both, the propagation constants $\gamma_{\mathrm{b}p}$ and the associated field distribution $\{E_{\mathrm{b}p}, H_{\mathrm{b}p}\}$ of the bent slotted waveguide modes for a given vacuum wavelength λ. Owing to the lossy nature of these modes, their propagation constants are complex-valued and so are the associated effective indices which are defined as $n_{\mathrm{eff,\,b}p} = \gamma_{\mathrm{b}p}/k$, where k represents the wave number $k = 2\pi/\lambda$ (see Ref. [19] for further details).

2.3. Bent slotted - straight waveguide couplers

After having determined the mode structure of the bent slotted waveguides, we combine this with the mode structure of the straight waveguides for the analysis of the bent slotted - straight waveguide couplers which we have delineated in Fig. 1. For the subsequent discussions, we apply the spatial coupled-mode approach of Ref. [21] to the present situation and provide in Fig. 2 a more detailed representation of such a coupling region.

For a given wavelength λ, the spatial coupled-mode approach constructs the fields in the coupler region by using the modal solutions of the uncoupled constituent waveguides. Consequently, for the straight waveguides we use the well-known modal solutions [26] and for the bent slotted waveguide we employ the analytical model as described in Sec. 2.2 above together with an appropriate transformation from polar (r,θ) to Cartesian (x,z) co-ordinates that are better suited for representing the coupler geometry. Here $x = r\cos\theta$, and $z = r\sin\theta$. Explicitly, we use the modal solutions for the fields $\{E_{\mathrm{s}q}, H_{\mathrm{s}q}\}$ and associated propagation constant $\beta_{\mathrm{s}q}$ for straight waveguides with refractive index profiles $n_{\mathrm{s}}(x)$ (or, equivalently, relative permittivity profiles $\varepsilon_{\mathrm{s}}(x) = n_{\mathrm{s}}^2(x)$) in a non-magnetic system as

$$\begin{pmatrix} E_{\mathrm{s}q} \\ H_{\mathrm{s}q} \end{pmatrix}(x,z) = \begin{pmatrix} \tilde{E}_{\mathrm{s}q} \\ \tilde{H}_{\mathrm{s}q} \end{pmatrix}(x)\, \mathrm{e}^{-\mathrm{i}\beta_{\mathrm{s}q} z}. \tag{5}$$

The corresponding modal solutions for the fields $\{E_{\mathrm{b}p}, H_{\mathrm{b}p}\}$ and propagation constants $\gamma_{\mathrm{b}p}$ of bent slotted waveguides with refractive index profiles $n_{\mathrm{b}}(x,z)$ (or, equivalently, relative permittivity profiles $\varepsilon_{\mathrm{s}}(x,z) = n_{\mathrm{s}}^2(x,z)$) in non-magnetic systems are

$$\begin{pmatrix} E_{\mathrm{b}p} \\ H_{\mathrm{b}p} \end{pmatrix}(x,z) = \begin{pmatrix} \tilde{E}_{\mathrm{b}p} \\ \tilde{H}_{\mathrm{b}p} \end{pmatrix}(r(x,z))\, \mathrm{e}^{-\mathrm{i}\gamma_{\mathrm{b}p} R\theta(x,z)}, \tag{6}$$

where R is the bend radius as defined in Fig. 1, and $\theta = \tan^{-1}(z/x)$ is the polar angle corresponding to the radial position $r = \sqrt{x^2+z^2}$ [24].

At this point, we would like to recall our basic assumption (or approximation) that the couplers are adiabatic, i.e., we assume that we can ignore back reflections and can restrict ourselves to uni-directional wave propagation. As a result, from the above modal solutions, we retain only the forward propagating modes, i.e., for the geometry described in Fig. 2 we retain only those waveguide modes that propagate in the positive z-direction.

Within the frequency-domain coupled-mode theoretical approach, the interaction between the bent slotted waveguide and the straight waveguide is restricted to a coupling region defined by $[x_l, x_r] \times [z_i, z_o]$ (see Fig. 2). Outside this region the fields propagating in each waveguide are

#141007 - $15.00 USD Received 13 Jan 2011; accepted 11 Mar 2011; published 19 Apr 2011

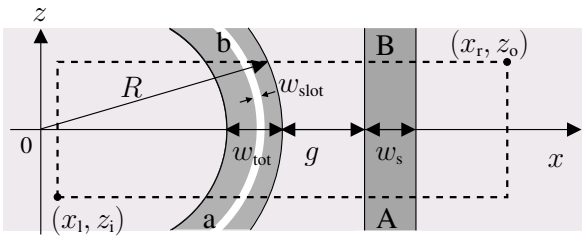

Fig. 2. Detailed representation of the bent slotted - straight waveguide couplers delineated in Fig. 1. The coupler is defined via the domain $[x_l, x_r] \times [z_i, z_o]$, in which the interaction between the bent slotted waveguide and the straight waveguide takes place. Outside this coupling region, we assume that the modes of the constituent waveguides are uncoupled. The minimal separation between the waveguides is g and the amplitudes of the input modes at $z = z_i$ are denoted by a and A, respectively. The corresponding amplitudes of the output modes at $z = z_0$ are denoted by b and B, respectively. See Fig. 1 for further details.

assumed to be uncoupled so that the individual modes propagate undisturbed according to their respective harmonic dependence. Within the coupler region, the corresponding fields $\{E,H\}$ are approximated by a superposition of the uncoupled modal fields, $\{E_{\mathrm{b}p}, H_{\mathrm{b}p}\}$ and $\{E_{\mathrm{s}q}, H_{\mathrm{s}q}\}$ of the forward propagation modes of the uncoupled bent slotted and straight waveguides, respectively. Explicitly, this reads as

$$\begin{pmatrix} E \\ H \end{pmatrix}(x,z) \approx \sum_{v=\mathrm{b,s}} \sum_{i=1}^{N_v} C_{vi}(z) \begin{pmatrix} E_{vi} \\ H_{vi} \end{pmatrix}(x,z) \tag{7}$$

with the *a priori* unknown, z-dependent amplitudes C_{vi}. Here, the index $v \in \{\mathrm{b,s}\}$ identifies the type of waveguide (b: bent slotted waveguide, s: straight waveguide) and the index i runs over the corresponding number of guided modes, i.e., $i = 1, \ldots, N_v$ and $v \in \{\mathrm{b,s}\}$.

We obtain the governing equations for $C(z) = \{C_{vi}(z)\}$ by combining the above ansatz (7) with the variational formulation of Maxwell's equations

$$\mathscr{F}(E,H) = \iint \left[(\nabla \times E) \cdot H^* - (\nabla \times H) \cdot E^* + \mathrm{i}\omega\mu_0 H \cdot H^* + \mathrm{i}\omega\varepsilon_0 \varepsilon E \cdot E^* \right] dx\,dz. \tag{8}$$

In the above equation, the stationarity of the functional $\mathscr{F}(E,H)$ implies that E and H satisfy Maxwell's curl equations $\nabla \times E = -\mathrm{i}\omega\mu_0 H$ and $\nabla \times H = \mathrm{i}\omega\varepsilon_0\varepsilon E$. Following the usual variational arguments [21], we arrive — as a necessary condition for the stationarity of the variational formulation — at the coupled-mode equations

$$\sum_{v=\mathrm{b,s}} \sum_{i=1}^{N_v} \mathsf{M}_{vi,wj} \frac{\mathrm{d}C_{vi}}{\mathrm{d}z} - \sum_{v=\mathrm{b,s}} \sum_{i=1}^{N_v} \mathsf{F}_{vi,wj} C_{vi} = 0, \tag{9}$$

for all $j = 1, \ldots, N_w$, and $w \in \{\mathrm{b,s}\}$. In the above equation, we have introduced the abbreviations $\mathsf{M}_{vi,wj}(x,z) = \int e_z \cdot \left(E_{vi}(x,z) \times H^*_{wj}(x,z) + E^*_{wj}(x,z) \times H_{vi}(x,z) \right) \mathrm{d}x$, and $\mathsf{F}_{vi,wj}(x,z) = -\mathrm{i}\omega\varepsilon_0 \int (\varepsilon(x,z) - \varepsilon_{vi}(x,z)) E_{vi}(x,z) \cdot E^*_{wj}(x,z)\,\mathrm{d}x$, where e_z denotes the unit vector in z-direction, the superscript '$*$' stands for complex conjugation, and $\varepsilon(x,z)$ represent the full relative permittivity profile for the entire coupler region. For a given value of z, the integration is carried out over the pre-defined coupler region in x-direction $[x_l, x_r]$.

Upon rewriting the coupled-mode equations [Eq. (9)] in matrix form, we obtain

$$\mathsf{M}(z) \frac{\mathrm{d}C(z)}{\mathrm{d}z} = \mathsf{F}(z)\, C(z). \tag{10}$$

#141007 - $15.00 USD Received 13 Jan 2011; accepted 11 Mar 2011; published 19 Apr 2011

Next, we define the transfer matrix $\mathsf{T}(z_j)$ at $z = z_j$ which connects the unknown amplitudes C at the position $z = z_i$ with the amplitudes at position $z = z_j$ according to $C(z_\mathrm{j}) = \mathsf{T}(z_j)\,C(z_\mathrm{i})$. By exploiting the linearity of Eq. (10) with respect to C, we may thus reformulate the problem in terms of the transfer matrix $\mathsf{T}(z)$ as a set of coupled differential equations

$$\frac{\mathrm{d}\mathsf{T}(z)}{\mathrm{d}z} = \mathsf{M}(z)^{-1}\,\mathsf{F}(z)\,\mathsf{T}(z), \tag{11}$$

with initial condition $\mathsf{T}(z_\mathrm{i}) = \mathsf{I}$. Here, I denotes the identity matrix. Upon solving Eq. (11) on an *a priori* defined domain $[x_l, x_r] \times [z_i, z_o]$ via standard integrators (we typically use a fourth-order Runge-Kutta method), we determine the transfer matrix $\mathsf{T}(z_o)$, which gives the coupler's output amplitudes $C(z_o)$ at position $z = z_o$ in terms of the coupler's input amplitudes $C(z_\mathrm{i})$ at position $z = z_\mathrm{i}$ according to $C(z_\mathrm{o}) = \mathsf{T}(z_o)\,C(z_\mathrm{i})$.

Projection corrections

At this point, we would like to note that the above coupler analysis is carried out on an *a priori* defined coupler domain $[x_l, x_r] \times [z_i, z_o]$. For a meaningful simulation of these coupler regions, it is essential to make sure that the coupler domain is appropriately selected. By examining the spatial extent of the mode profiles of the constituent waveguide modes in the direction normal to the waveguides, we can straightforwardly determine an appropriate length of the coupler domain in x-direction $[x_l, x_r]$ (see the mode profiles depicted in Fig. 4).

However, obtaining an estimate for the length of the coupler domain in z-direction is less straightforward. A choice of $[z_i, z_o]$ will be justified, if the corresponding simulation results validate the assumption that the modes of the constituent waveguides are uncoupled outside the coupler domain. In order to verify this numerically, we consider a system where only the fundamental mode of the straight waveguide is excited, i.e., $C(z_\mathrm{i}) \equiv 0$ except for $C_{\mathrm{s}0}(z_\mathrm{i}) = 1$. Then by matching the fields at the output position $z = z_o$, we determine the amplitudes of the straight waveguide modes $B = C(z_\mathrm{o})$. Keeping $z = z_i$ fixed and varying the other end $z = z_o$, allows us to monitor the evolution of the straight waveguide's fundamental mode amplitude $B_{\mathrm{s}0}$. If the assumption of uncoupled modes is satisfied, we expect that this amplitude's absolute value $|B_{\mathrm{s}0}| = |C_{\mathrm{s}0}(z_\mathrm{o})|$ attains a stationary value.

In Fig. 3, we display the results of a corresponding computation. For this field matching procedure, we observe a strong oscillatory behavior of $|B_{\mathrm{s}0}|$ even for relatively large values of z_o (dashed lines). Although, these oscillations will eventually be damped out for large values z_o, this would lead to undesirably large coupler domains. Therefore, the 'naive' field-matching approach described above is rather unsatisfactory, and we should not directly use the transfer matrix $\mathsf{T}(z_o)$ as the required coupler scattering matrix S for the CMT model described in Sec. 2.1.

A more efficient approach utilizes a projection of the complete field distribution inside the coupler onto the modes of the uncoupled straight waveguide in order to extract the amplitude $B_{\mathrm{s}0}$ and all other amplitudes. In Fig. 3, we also display the results of this projection technique (solid line) and observe a superior performance relative to the naive field matching technique (dashed line). For a detailed explanation of this projection technique and reasoning behind its effectiveness we would like to refer the reader to Ref. [21]. Here, we only would like to point out that this projection operation is essential for obtaining stable results for the amplitudes of the straight and bent slotted waveguides modes outside the coupler domain. In addition, the corresponding results (see solid line in Fig. 3) also validate the assumption of a finite coupler region in Sec. 2.1. Finally, we obtain the required coupler scattering matrix S by incorporating these projection corrections into the results of the transfer matrix $\mathsf{T}(z_o)$.

#141007 - $15.00 USD Received 13 Jan 2011; accepted 11 Mar 2011; published 19 Apr 2011

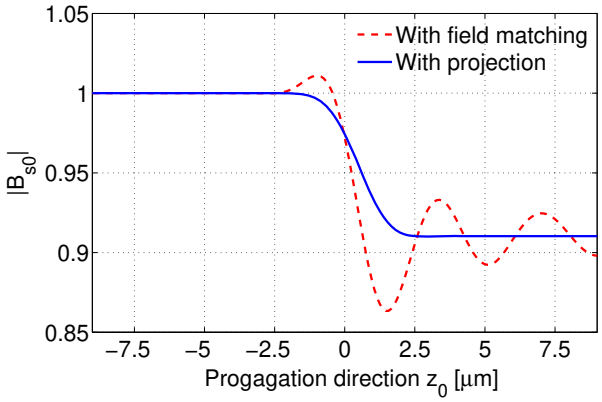

Fig. 3. Dependence of the straight output waveguide's fundamental mode amplitude B_{s0} on the coupler length in z-direction when the input straight waveguide is excited with its fundamental mode. These results have been obtained with the 'naive' field-matching approach (dashed line) and with the projection correction technique (solid line). The coupler parameters (see Fig. 2) are: $n_c = n_s = 2.1$, $n_{slot} = n_b = 1$, $w_{tot} = 1\ \mu$m, $w_{slot} = 0.2\,\mu$m, $w_s = 0.4\ \mu$m, $\lambda = 1.55\ \mu$m, $g = 0.4\ \mu$m, $\eta = 0.5$, $R = 5\ \mu$m, $[x_l, x_r] = [1\,\mu\text{m}, 8\,\mu\text{m}]$, $z_i = -8\,\mu$m is fixed, and z_o is varied from $[-8\,\mu\text{m}, 8\,\mu\text{m}]$. The numerical computations have been performed with discretizations $h_x = 0.005\,\mu$m and $h_z = 0.1\,\mu$m along the x- and z-directions respectively.

2.4. Evaluation of the spectral response

By following the procedures in Secs. 2.2 and 2.3 we can compute the bent slotted waveguide propagation constants and the coupler scattering matrices for a given wavelength λ. Via a subsequent evaluation of the expressions [Eq. (4)], we can then compute the complete response of the slotted-resonator device at that wavelength. Upon repeating this procedure for a series of wavelengths, we can determine the entire spectral response of the device with considerably reduced effort relative to a full-fledged exact numerical simulation. In order to further reduce the computational efforts within the CMT approach, we employ a speed-up technique which is based on analytical arguments and interpolation.

More precisely, the (original) scattering matrix obtained in Sec. 2.3 exhibits fast oscillations when the wavelength is varied and, therefore, is ill-suited for an interpolation between wavelengths. However, by separating these oscillations into fast oscillations (which are mainly due to phase changes in the mode propagation) and slow oscillations (which are mainly due to the coupling effects), we can construct a modified scattering matrix that is suitable for interpolation (see Ref. [21] for details). In practice, we perform the complete coupled-mode based computations for the bent slotted waveguide's propagation constants and the coupler scattering matrices only at pre-selected nodal wavelengths. Then, we determine the parameters that are required for intermediate wavelengths via cubic interpolation and, again, utilize expressions [Eq. (4)] in order to evaluate the device characteristics. All the subsequent CMT-based computations utilize this highly efficient speed-up technique. If the desired wavelength interval contains only a few resonances (as in our case, e.g. see Fig. 5), then no special consideration is required for a selection of nodal wavelengths. Otherwise, as one expects from the increasing interpolation errors away from the nodal points, the interpolated spectral results are reliable only in the vicinity of the nodal wavelengths.

#141007 - $15.00 USD
Received 13 Jan 2011; accepted 11 Mar 2011; published 19 Apr 2011

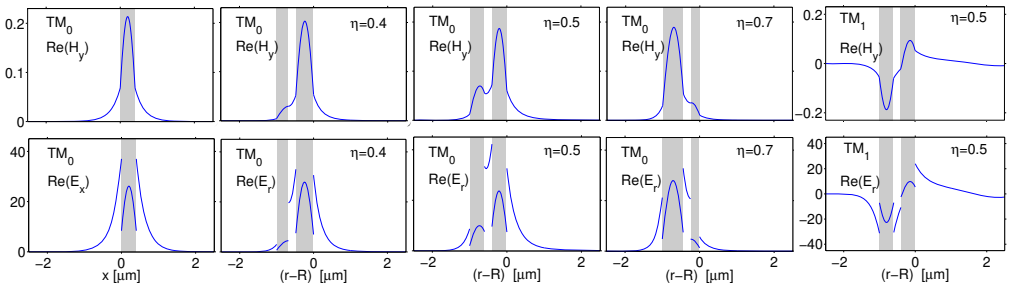

Fig. 4. Transverse profiles of selected waveguide modes that are used for the CMT-based simulations of the couplers in Sec. 2.3. The first column depicts the real part of H_y and E_x for the straight waveguide TM_0 mode. The TM_0 modes of the bent slotted waveguides for various values of η are depicted in the second, third and fourth column (see inset). The fifth column depicts the TM_1 mode for the bent slotted waveguide for $\eta = 0.5$. All these modes are computed at $\lambda = 1.55\,\mu$m, and the corresponding effective indices are (columnwise) $n_{\rm eff}$=1.4335343, $1.53462 - \mathrm{i}\ 3.50971 \times 10^{-8}$, $1.4221 - \mathrm{i}\ 2.92095 \times 10^{-6}$, $1.48579 - \mathrm{i}\ 8.3777 \times 10^{-9}$, and $1.19039 - \mathrm{i}\ 1.69572 \times 10^{-3}$ respectively.

3. Simulation results

As an illustration of our CMT approach to slotted resonator devices, we consider a specific system: A micro-ring of radius $R = 5\,\mu$m and width $w_{\rm tot} = 1\,\mu$m which is made of silicon nitride (refractive index $n_{\rm c} = 2.1$) is micro-structured to exhibit a slot of width $w_{\rm slot} = 0.2\,\mu$m that is filled with air (refractive index $n_{\rm slot} = 1$). As depicted in Fig. 1, the position of the slot inside the ring resonator is controlled by the asymmetry parameter η. This slotted ring resonator is coupled to two identical straight silicon-nitride waveguides (refractive index $n_{\rm s} = 2.1$) that are $w_{\rm s} = 0.4\,\mu$m wide. The minimal separation between these bus waveguides and the ring resonator is $g = \tilde{g} = 0.4\,\mu$m. Finally, we assume that the entire device is placed in an air background (refractive index $n_{\rm b} = 1$) and study its spectral response in the wavelength range $[1.5\,\mu\mathrm{m}, 1.6\,\mu\mathrm{m}]$. For these settings, the uncoupled straight waveguide is mono-modal, whereas for the uncoupled bent slotted waveguide we have to take into account all the modes which exhibit a real part of their effective index that is above 'cutoff', i.e., for which $\Re(n_{\rm eff}) \geq n_{\rm b}$. We have found that for the above settings this corresponds to the fundamental and the first-order mode.

In Fig. 4, we display characteristic transverse profiles of some of these modes for different slot positions within the ring resonator, i.e., for several different values of η. The corresponding properties of the bent slotted waveguide modes strongly depend on the slot's position. In particular, the first-order TM_1 mode is moderately lossy only if the slot is symmetrically positioned within the ring ($\eta = 0.5$). For instance, at $\lambda = 1.55\,\mu$m, we obtain its effective index $n_{\rm eff} = 1.19039 - \mathrm{i}\ 1.69572 \times 10^{-3}$. For the first-order mode, asymmetric positions of the slot either lead to a very lossy mode or a mode located close to 'cutoff'. For instance, at $\lambda = 1.55\,\mu$m for TM_1 we obtain for $\eta = 0.4$ an effective index $n_{\rm eff} = 1.09129 - \mathrm{i}\ 9.96678 \times 10^{-3}$ and for $\eta = 0.7$ we find $n_{\rm eff} = 1.13048 - \mathrm{i}\ 1.49073 \times 10^{-2}$.

With these modes, we simulate the couplers on the domain defined by $[x_l, x_r] = [1\,\mu\mathrm{m}, 8\,\mu\mathrm{m}]$ and $[z_i, z_o] = [-3\,\mu\mathrm{m}, 3\,\mu\mathrm{m}]$ by using discretizations of $h_x = 0.005\ \mu$m and $h_z = 0.1\ \mu$m along the x- and z-direction, respectively. Following the procedure outlined in Sec. 2.4, we calculate the spectral response of the slotted resonator over the entire wavelength range $[1.5\,\mu\mathrm{m}, 1.6\,\mu\mathrm{m}]$ via a cubic interpolation technique that utilizes computations at the nodal wavelengths $1.5\,\mu$m, $1.55\,\mu$m, and $1.6\,\mu$m.

#141007 - $15.00 USD Received 13 Jan 2011; accepted 11 Mar 2011; published 19 Apr 2011

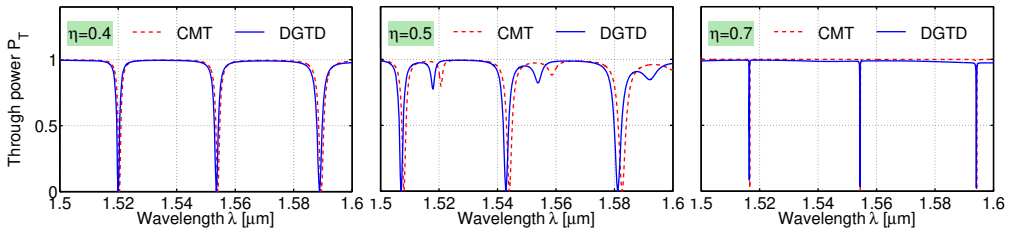

Fig. 5. Spectral response of the slotted resonator device depicted in Fig.1 for the TM polarization and various slot positions within the ring (see the text for details on the device parameters). The results of the coupled-mode theoretical (CMT) approach are compared with the results of exact numerical computations via a Discontinuous Galerkin Time-Domain (DGTD) method that has been equipped with curvilinear elements.

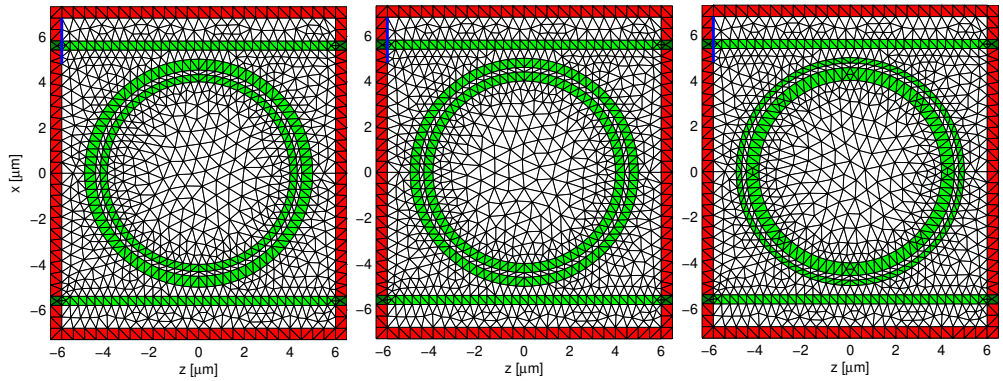

Fig. 6. Meshes that have been used for the DGTD computations of the slotted resonator device sketched in Fig. 1. From left to right, the slot position corresponds to $\eta = 0.4$, $\eta = 0.5$, and $\eta = 0.7$ respectively. The computational domain is enclosed by perfectly matched layers as indicated by the finite-width outermost box. In order to determine the spectral response of the device a broad-band pulse for is injected in the upper left waveguide. The flux through the output ports is recorded and subsequently Fourier-transformed.

In Fig. 5, we display the resulting spectral response of the slotted resonator device for TM-polarized mode and various values of the asymmetry parameter η. In particular, each dip in the through-power P_T corresponds to a particular $TM_{n,m}$ cavity mode resonance of the slotted resonator, where the indices n and m denote radial and angular mode number, respectively. The prominent sharp dips correspond to the resonances of the fundamental cavity modes $TM_{0,m}$ and they exhibit wildly varying quality factors (see discussion below). In addition, for the symmetric case $\eta = 0.5$, we also find further secondary dips, which, in general, correspond to higher-order cavity modes — in the particular case we are considering — they correspond to the first-order $TM_{1,m}$ modes. Consistent with our discussion above, we find that in the case of $\eta = 0.4$ and $\eta = 0.7$, the TM_1 bent slotted waveguide modes are very lossy and, therefore, fail to appreciably contribute to the overall spectral response of the device.

In order to assess the validity and accuracy of the coupled-mode approximations discussed above, we have compared the CMT results with those obtained from a Discontinuous Galerkin Time-Domain (DGTD) method [4–7]. We have chosen this particular method because of its ability to employ unstructured meshes in conjunction with high-order spatial basis functions.

#141007 - $15.00 USD
Received 13 Jan 2011; accepted 11 Mar 2011; published 19 Apr 2011

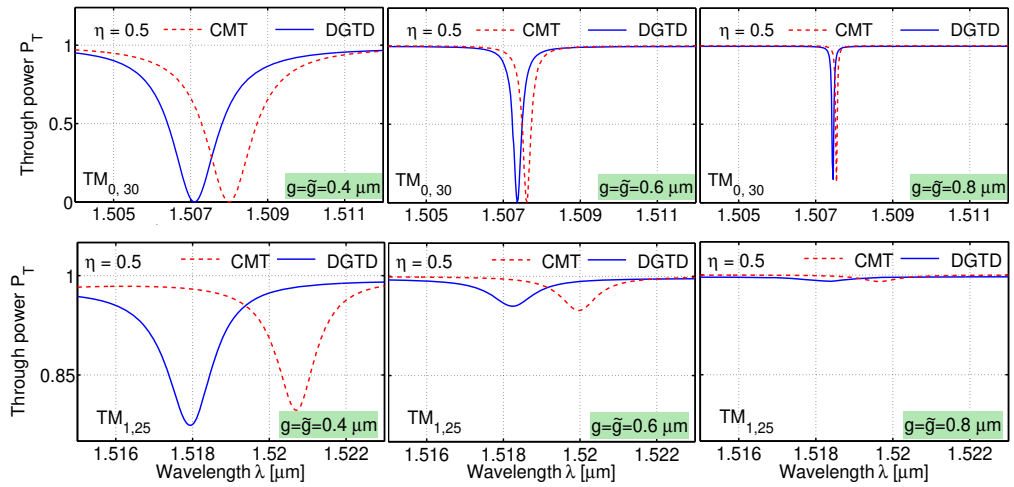

Fig. 7. Spectral response of the slotted resonator device depicted in Fig. 1 for a symmetric slot position ($\eta = 0.5$) for various minimal separations g and $\tilde{g}$ of the straight waveguides from the slotted resonator (see the text for details on the device parameters). The results of the coupled-mode theoretical (CMT) approach are compared with the results of exact numerical computations via a Discontinuous Galerkin Time-Domain (DGTD) method that has been equipped with curvilinear elements.

These features allow to properly resolve the fields in the sub-wavelength slot and to handle the discontinuous fields without requiring unreasonable simulation times. In contrast to earlier computations of similar systems [6], we have equipped the DGTD method with curvilinear elements which provides an excellent representation of the true ring geometry. In Fig. 6, we depict the corresponding meshes used for the DGTD computations.

In all of our subsequent DGTD computations we have utilized a spatial expansion order of $p = 6$ (see Ref. [5]). For time-stepping, we have used a suitably selected fourth-order low-storage Runge-Kutta scheme. At this point, we would like to note that we have carried out extensive convergence studies with higher and lower spatial discretization orders. In addition, we have compared the CMT and DGTD spectra with results from computations based on the freely available FDTD implementation meep [27]. From those studies and comparisons, we can safely conclude that our DGTD results are accurate to at least four significant digits. Upon comparing the spectra of CMT and DGTD computations (see Fig. 5) we observe reasonable agreement for the fundamental resonances. However and notably for the symmetric case of $\eta = 0.5$, the CMT and DGTD results differ significantly for the lossy first-order resonances.

This discrepancy can be explained as follows. As mentioned in Secs. 2.1 and 2.3, the CMT model of the resonator assumes that the constituent bent slotted - straight waveguide couplers are adiabatic, so that the field propagating in one part of the coupler experiences a slowly increasing presence of the other waveguide. Based on this, we have assumed uni-directional wave propagation, and the set of *a priori* unknown coupled mode amplitudes C_{vi} in Eq. (7) are assumed to be z-dependent only. These assumptions are violated if the modes of the bent slotted waveguides are not anymore well confined to the waveguide core (e.g., the TM_1 bent slotted waveguide mode displayed in Fig. 4) and the constituent waveguides in the coupler are not sufficiently separated. Therefore, we expect that increasing the minimal coupler separations, g and $\tilde{g}$, leads to an improvement of the CMT model's accuracy, notably regarding the secondary resonances associated with the first-order modes. In order to validate this reasoning, we

#141007 - $15.00 USD Received 13 Jan 2011; accepted 11 Mar 2011; published 19 Apr 2011

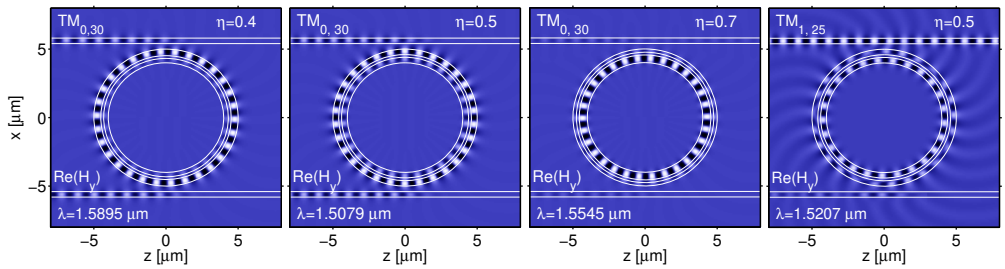

Fig. 8. Resonance field distributions (real part) of the magnetic field H_y of the slotted resonator device depicted in Fig. 1 for various values of the asymmetry parameter η (see the text for details on the device parameters). The three leftmost panels depicts the resonator's $TM_{0,30}$ resonances for $\eta = 0.4$, $\eta = 0.5$, and $\eta = 0.7$, respectively. The rightmost panel depicts the resonator's $TM_{1,25}$ resonance for $\eta = 0.5$. These field distributions have been obtained with the CMT model.

have computed the spectral response of the symmetric slotted resonator device ($\eta = 0.5$) for larger values of the minimal separations g and $\tilde{g}$, and display the results in Fig. 7. Indeed, we find that the discrepancy between the results of the CMT model and the DGTD computations are strongly reduced for larger values of the separation. These results provide a very reliable method for determining the validity and/or accuracy of the adiabatic coupling assumption of the coupled-mode approach.

In order to obtain a better perspective of the various resonances appearing in Fig. 5, we have also determined the corresponding field distributions. Specifically, we have traced the slotted resonator's $TM_{0,30}$ resonance as the asymmetry parameter η is varied and display the results in Fig. 8. We observer that, for $\eta = 0.4$, the principal field component H_y is neatly localized in the outer high-index layer of the ring cavity. When the slot is placed symmetrically within the core of the ring, i.e., when $\eta = 0.5$, we still observe a significant localization of the magnetic field H_y in the outer high-index ring. However, we cannot anymore neglect the magnetic field in the inner ring. For even higher values of, say, $\eta = 0.7$, the magnetic field is predominantly localized in the inner high-index layer of the ring. This strong confinement of the field is the primary reason for the sharp resonances which we have observed for $\eta = 0.7$ as compared to the resonance for $\eta = 0.4, 0.5$.

The sharpness of these resonances is measured in terms of the quality factor Q, which is defined as a ratio of the central resonance wavelength to the full-width-at-half-maximum value. The corresponding Q-values of this $TM_{0,30}$ resonance for $\eta = 0.4, 0.5$, and 0.7 are approximately 900, 1200, and 26000 respectively. This demonstrates that a careful positioning of the slot is of particular importance when cavities with high quality factors are desired. Finally, in the far-right panel of Fig. 8 we depict the field distribution that corresponds to the (weak) secondary resonance of the slotted resonator's $TM_{1,25}$ mode for $\eta = 0.5$. Due to the lossy nature of this mode, the field is only weakly confined and a considerable amount of the field resides outside the actual cavity.

4. Conclusions

In conclusion, we have developed a CMT approach for slotted-resonator based systems. For a two-dimensional model problem we have compared its accuracy with exact numerical computations based on a DGTD solver. In particular, within the CMT approach we decompose the system into input and output ports, connecting waveguide segments, and couplers between the different types of uncoupled waveguides. For these uncoupled waveguides, we utilize analyti-

#141007 - $15.00 USD
Received 13 Jan 2011; accepted 11 Mar 2011; published 19 Apr 2011

cally available results and for the description of the coupler, we use the corresponding modes as an expansion basis for the fields. The corresponding expansion coefficients are determined via a variational formulation that utilizes an adiabatic approximation and allows us to define an appropriate transfer matrix. Using a projection correction, we then determine the coupler's scattering matrix. Finally, we combine these ingredients along with an interpolation speed-up technique into a framework that allows us to determine the spectral response of the slotted resonator device with just a few computations.

For truly adiabatic coupling, the comparison of the CMT model with the rigorous direct numerical simulation results of the DGTD approach shows very good agreement. In addition, the CMT model provides considerable insight into the underlying physical mechanisms based on the properties of the various waveguiding modes. In particular, we have found that the exact location of the slot within the resonator has a strong influence on the quality factor of the resonances. In turn, this provides valuable information for the design of optimized sensor configurations and nonlinear optics applications.

While we have demonstrated the working of the CMT model in a two-dimensional framework, there is no conceptual difficulty in extending the CMT model to 3D systems. This has, for instance, already been demonstrated in Ref. [28] for conventional micro-resonators. The CMT model thus forms a convenient basis for the efficient analysis of more complex systems that contain slotted resonators and/or slotted waveguides. For instance, we anticipate that entire arrays of coupled waveguide-resonator systems, arrays of coupled resonators and systems with strongly nonlinear optical properties can be treated within the above CMT approach. In addition, an extension of the CMT model to plasmonic resonators, photonic-crystal based resonators and waveguiding structures is conceivable.

Acknowledgment

This work is partially funded by the Deutsche Forschungsgemeinschaft (DFG) through the DFG Research Training Group 1294 'Analysis, Simulation and Design of Nanotechnological Processes' at the Karlsruhe Institute of Technology (KIT). We further acknowledge financial support by the DFG and the State of Baden-Württemberg through the DFG-Center for Functional Nanostructures (CFN) within subprojects A1.2 and A5.6. The research of J.N. is supported by the Young Investigator Group (YIG) program of KIT. The simulations in the present work use the slab straight waveguide mode solver developed and generously shared by Manfred Hammer (University of Twente). We acknowledge support by DFG and Open Access Publishing Fund of KIT.

#141007 - $15.00 USD Received 13 Jan 2011; accepted 11 Mar 2011; published 19 Apr 2011